Available online at www.sciencedirect.com
SCIENCE DIRECT®
Continental Shelf Research 26 (2006) 269–282
CONTINENTAL SHELF RESEARCH
www.elsevier.com/locate/csr

Composition and flux of groundwater from a California beach aquifer: Implications for nutrient supply to the surf zone

Alexandria B. Boehm[a,*], Adina Paytan[b], Gregory G. Shellenbarger[c], Kristen A. Davis[a]

[a]*Department of Civil and Environmental Engineering, Environmental Water Studies, Stanford University, Stanford, CA 94305, USA*
[b]*Department of Geological and Environmental Sciences, Stanford University, Stanford, CA 94305, USA*
[c]*SG Science, 401 13th Street, Sacramento, CA 95814, USA*

Received 9 December 2004; received in revised form 22 November 2005; accepted 23 November 2005

Abstract

The coastal, unconfined aquifer at Huntington Beach, California contains saline groundwater (33 psu) adjacent to the water line, and a brackish groundwater (BGW) mixing zone (3–9 psu) approximately 50 m from the water line. According to salinity and water isotope analyses, the BGW composition varies spatially in the alongshore direction. Measurements obtained from two BGW wells indicate this water is a mixture of seawater and a freshwater end member (likely infiltrated runoff); results from a third more southerly well suggest the BGW is composed of seawater, freshwater, and water from the confined Talbert Aquifer. Saline groundwater, on the other hand, shares similar salinity and water isotopic composition with seawater. The saline groundwater is enriched with short- and long-lived radium isotopes relative to the surf zone, which in turn is enriched relative to waters further offshore. We derive eddy diffusion coefficients for the nearshore using ^{223}Ra and ^{224}Ra, and in conjunction with ^{226}Ra activities, estimate a submarine groundwater discharge (SGD) rate between 4.2 and 8.9 L min^{-1}m^{-1} of shoreline, respectively. Using analytical models, we estimate that between 74 and 100% of this discharge represents seawater than has been forced by tides and waves through the beach aquifer. Under one set of model assumptions, results indicate that a portion (up to 56%) of seawater pumped into the beach aquifer by waves and tides is not discharged suggesting salt water intrusion may be occurring. Because saline groundwater is enriched with dissolved inorganic nitrogen and soluble reactive phosphate relative to the coastal ocean, our results suggest that tidally and wave-driven seawater circulated through the beach aquifer represents an important mechanism for nutrient input to the nearshore environment in dry weather. Estimates of nutrient flux to the coastal ocean via SGD along 16–17 km of shoreline are equivalent to nutrient fluxes from two salt water wetlands near the study site during the dry season.

Keywords: Surf zone; Groundwater; Nutrient; Radium isotopes; Beach aquifer; Water isotopes, USA; California; Huntington beach

1. Introduction

Over the last two decades, researchers have come to recognize that submarine groundwater discharge (SGD, defined as the combined mixture of freshwater and recirculated seawater discharging to the

*Corresponding author. Tel.: +650 724 9128.
E-mail address: aboehm@stanford.edu (A.B. Boehm).

0278-4343/$ - see front matter © 2005 Elsevier Ltd. All rights reserved.
doi:10.1016/j.csr.2005.11.008

ocean from a coastal aquifer) can be a significant contributor of nutrients and freshwater to the coastal environment under certain conditions (Johannes, 1980; Valiela et al., 1990; Krest et al., 2000; Paytan et al., 2006; Shellenbarger et al., in review). Locally, groundwater inputs to the coastal zone can have major effects on geochemical cycles either through the discharge of fresh groundwater or the recirculation of seawater through shoreline aquifers (Buddemeier, 1996; Moore, 1997, 1999). SGD is now recognized as a potentially important pathway for pollution migration to the nearshore, particularly where agricultural or urban activities have impacted the groundwater (Cable et al., 1996; Corbett et al., 1999, Kelley and Moran, 2002; Boehm et al., 2004). Because 37% of the world's population lives within 100 km of the coastal zone (Cohen et al., 1997), understanding the increasing effects of the ever-growing human population on the coastal environment is critical to development of sound management principles.

Moore (1999) characterizes the subsurface landward of the land–sea interface as a subterranean estuary where water is exchanged between the sea and aquifers. Tidal pumping of seawater through the beach aquifer causes constant inflow to and outflow from the beach aquifer (Nielson, 1990). Wave pumping also contributes to infiltration and discharge over shorter time scales than the tides (Longuet–Higgens, 1983). Terrestrial flows resulting from aquifer recharge, as well as seasonal exchange of saline groundwater and dispersive entrainment of saline groundwater along the freshwater–saltwater interface in the beach aquifer also drive exchange (Michael et al., 2005). The result of these processes is constant mixing and exchange of groundwaters of both terrestrial and marine origin, along with the interaction of these waters with aquifer substrate (rocks, sand, or sediment) (Church, 1996). In this study, we use the term SGD to describe groundwater of both terrestrial and marine origins.

The four naturally occurring radium isotopes, which vary in half-life (3.7 days to 1600 years), are useful as tracers of SGD and have also been used to study groundwater input and mixing processes on a wide range of time scales (Elsinger and Moore, 1983; Moore, 1997; Yang et al., 2002; Charette et al., 2001; Krest and Harvey, 2003). The divalent cation radium isotopes are bound to soil particles and rocks in low ionic strength water. They readily desorb via ion exchange in the presence of solutions of high ionic strength (e.g., Elsinger and Moore, 1983; Webster et al., 1994; Yang et al., 2002). In coastal aquifers where seawater with high ionic strength mixes and interacts with freshwater and aquifer rocks, respectively, high radium waters can result. On the other hand, open ocean seawater has relatively low radium activities. Therefore, excess radium in the coastal ocean (over the offshore seawater activities) suggests a coastal source that in many cases is the unconfined surficial aquifer (Moore, 1996, 2003; Moore et al., 2002).

In a previous study (Boehm et al., 2004), we used short-lived radium isotopes ^{223}Ra and ^{224}Ra as tracers of SGD at Huntington Beach, California (Fig. 1) and investigated the correlation of SGD with microbial pollution in the surf zone. However, the study did not demonstrate to what extent the water in the coastal unconfined aquifer and SGD was composed of tidally and wave-pumped re-circulated seawater, meteoric water, water originating in a confined aquifer, or seawater pumped via other forcing mechanisms (Michael et al., 2005). Fig. 2 illustrates a conceptual model of the rock–water interactions in the subsurface of the field site, illustrating the potential contributions to SGD and beach groundwater. In the current study, we introduce new measurements of ^{226}Ra (half-life of 1600 yr) and isotopic ratios of hydrogen and oxygen from coastal waters and groundwater. The purposes of this study are to (1) explore the origin of the groundwater within the unconfined beach aquifer

Fig. 1. Map of the field site. Background is from the USGS seamless database. TA is the location of the Talbert Aquifer well sample, TM is the mouth of the Talbert Marsh, SAR is the mouth of the Santa Ana River, stations 7 through 11 are sampling sites. Stations 9 and 10 represent the primary study area.

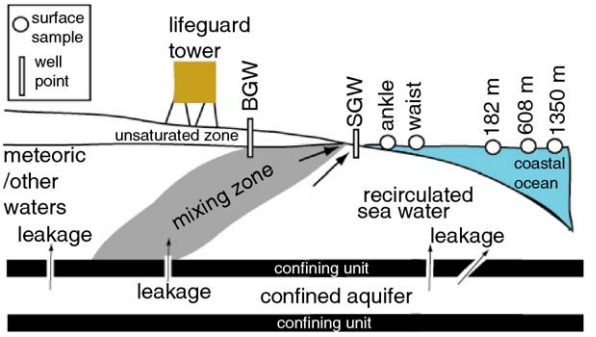

Fig. 2. Conceptual model of the beach aquifer at the field sites. Hypothetical breaches in the confining unit between the confined and unconfined aquifer are shown where vertical leakage could occur. Locations where sampling occurred are also shown and labeled. SGW and BGW are saline and brackish groundwater, respectively, and are described in detail in the text in terms of their salinity. Arrows represent the direction of actual or hypothetical water flow.

and SGD, (2) determine the groundwater discharge rates to the coastal ocean using cross-shore eddy diffusivity coefficients derived from short-lived radium isotope activities (to compare to previous results obtained by a mass balance box model), and (3) apply the models of wave-driven groundwater circulation of Longuet-Higgens (1983) and tidally pumped groundwater circulation of Nielson (1990) to the study site to determine the proportions of SGD that result from wave and tidal pumping of seawater, and the proportion that is due to discharge of others waters (e.g., meteoric, water leaking from the confined aquifer, or seawater discharged under other forces).

2. Material and methods

2.1. Field sampling: surf zone

Four 3-day sampling excursions were conducted during the summer of 2003 during two neap tides and two spring tides. Two low tides and two high tides were sampled for a total of four sampling events during the majority of the sampling excursions. During each event, seawater was collected from the near surface of the surf zone in ankle and waist deep water adjacent to lifeguard stations 9 (33°38.327 N, 117°58.577 W) and 10 (33°38.416 N, 117°58.725 W) (Figs. 1 and 2). In addition, during each low tide, a groundwater sample was obtained from the unconfined aquifer by pumping from a shallow well (<1 m deep) in the intertidal zone, far enough from the swash zone so that no surface water contaminated the well. We also obtained (1) surface seawater samples from approximately 182, 608, and 1350 m offshore of station 9 during a neap and spring tide at low tide in conjunction with nearshore and groundwater sampling and (2) groundwater from shallow wells (<1 m deep) in the intertidal zone and seawater from the near surface of the surf zone at knee depth at stations 7, 8, and 11 (Figs. 1 and 2) during low tide under spring and neap tide conditions. All seawater samples were collected from a vertically well-mixed water column based on previous characterization of stratification in the nearshore (Boehm et al., 2002).

2.2. Field sampling: other locations

To characterize other potential local water sources to the surf zone, we collected samples during spring and neap tidal conditions at the mouths of the Santa Ana River and Talbert Marsh when the tide was ebbing as well as groundwater from the Talbert Aquifer (TA in Fig. 1), a confined aquifer managed by the Orange County Water District (OCWD). The aquifer sample was collected from a well (#M31, OCWD) screened between 25 and 50 m deep, located 1000 m inland from our study site.

Samples from the mixing zone in the unconfined aquifer (located approximately 50 m from the mean low water line) were collected using screened PVC well-points. These were installed using a hand auger at stations 8, 9, and 10 (Figs. 1 and 2). Screens were positioned within the top 1 m of the aquifer, which was located approximately 3 m below the surface of the sand. A total of four groundwater samples were pumped from each well during two low tides and two high tides starting 12 h after well-point installation. Prior to sample collection, wells were purged for 5 min.

We obtained a sample of fresh groundwater (salinity < 1 psu) from the surficial aquifer at station 9 during August 2005. Although not collected contemporaneously with the rest of the water samples, the fresh groundwater sample potentially represents a fresh end member in the surficial aquifer. The sample was obtained in the same manner as water from the mixing zone using a PVC well point installed approximately 60 m from the mean low water line. The single fresh groundwater sample was processed only for $\delta^{18}O$ for inclusion in a mixing diagram. Salinity was measured using a

conductivity/temperature probe (YSI 30, Yellow-springs, OH). The limitations of including this sample in our analysis are discussed in the Results section.

All samples obtained during these studies (unless otherwise stated) were analyzed for ^{226}Ra activities and salinity as described below. A subset of the samples were analyzed for water isotopic composition. ^{223}Ra and ^{224}Ra activities as well as nutrient concentrations (nitrate, ammonium, and soluble reactive phosphate (SRP)) for these samples were reported by Boehm et al. (2004).

2.3. Water analyses: radium isotopes

95, 76, and 38 L of water were collected for seawater, brackish groundwater (BGW), and saline groundwater (SGW) samples, respectively. Water was passed over manganese-impregnated acrylic fibers at a flow rate $\leqslant 1.5\,\mathrm{L\,min^{-1}}$ in the field immediately after collection (Moore, 1976). Plugs of untreated acrylic fiber were placed in the column to reduce the deposit of sediment and plankton from the sample on the impregnated acrylic fibers.

^{226}Ra activity was quantified using a Rad7 (Durridge Co. Inc., Bedford, MA) following the method described by Kim et al. (2001). This method provides quantification of ^{218}Po, the daughter of ^{222}Rn (a ^{226}Ra daughter). Fibers were moistened with MilliQ water to obtain constant recoil efficiency for radon, placed into air tight glass tubes, flushed with helium, and incubated for approximately three weeks to allow ingrowth of ^{222}Rn and secular equilibrium to be achieved. Measurement precision estimated by multiple analyses of several gravimetrically prepared samples was within 10%.

2.4. Water analyses: δD and $\delta^{18}O$ of water

30 mL of 0.2 μm filtered water were sub-sampled from the large volume samples, immediately stored on ice, and then frozen. Water samples for analysis of hydrogen isotopic composition were prepared using zinc reduction (Kendall and Coplen, 1985). Water samples for analysis of oxygen isotopic composition were prepared by equilibration with CO_2 at 25 °C (Epstein and Mayeda, 1953). Values are reported per mille (‰) relative to Vienna Standard Mean Ocean Water (VSMOW). Precisions of δD and δ^{18}O are better than ± 1.0 and 0.05 ‰, respectively.

2.5. Water analyses: salinity

To obtain an accurate and precise estimate of salinity, 10 mL of water were sub-sampled from the large volume samples, filtered through a 0.2 μm filter, and stored at 4 °C for densiometric analysis (Anton-Paar model DMA 4500, Graz, Austria). Densities were converted to salinities with the UNESCO Equation of State (IES 80) (http://fermi.jhuapl.edu/denscalc.html). The precision of our salinity measurements are within 0.01 psu.

2.6. Sand analysis: hydraulic conductivity and porosity

The hydraulic conductivity of unconsolidated sand collected from the unconfined aquifer at the field site was assessed using a bench top combination permeameter (SOILTEST, Ele International, model K-605A, Pelham, Alabama). Because none of the sediment passed through a number 200 sieve, a constant head test was performed as per the manufacturer's directions. Two separate sand samples were tested using a range of configurations. A total of seven estimates was obtained, averaged, and compared to estimates obtained in situ within 1 km of the field site using aquifer pumping tests (Theis, Neuman and Distance-Drawdown methods, Komex H_2O Science, 2000). The comparison with in situ estimates was necessary because it is well understood that removing sand from an aquifer can change its hydraulic conductivity. The porosity was estimated by measuring the volume of water needed to fill the pore spaces in a predetermined volume of sand.

2.7. Modeling: mixing coefficient and seepage rate

The seepage rate of groundwater from the coast was calculated using the offshore gradient of ^{226}Ra and eddy diffusivity coefficients K inferred from the exponential decrease of ^{223}Ra and ^{224}Ra with distance from shore following Moore (2003). In brief, the slope (m) of the line describing the decline of ln ^{223}Ra or ln ^{224}Ra with distance in the offshore direction (x) can be used to estimate K as follows:

$$K = \lambda m^{-2}, \tag{1}$$

where λ is the tracer's decay constant (0.061 and 0.19 $\mathrm{day^{-1}}$ for ^{223}Ra and ^{224}Ra, respectively). K is then used to estimate the flux F of ^{226}Ra from

the shoreline:

$$F = -K\frac{dB}{dX}, \tag{2}$$

where dB/dx is the offshore gradient of ^{226}Ra. It should be noted that this model assumes no alongshore gradient in groundwater discharge, no net offshore advection, and steady-state conditions.

2.8. Modeling: wave-driven and tidally driven SGD

SGD, as calculated with ^{226}Ra gradients, is composed of fresh and saline groundwater discharge to the coastal ocean. The outflow portion of tide- and wave-pumped seawater circulation is included in SGD, although these do not contribute to net discharge over longer time scales that may occur as a result of aquifer recharge (Li et al., 1999). Thus, total SGD (D) can be expressed as $D = D_t + D_w + D_m$, where D_t and D_w represent outflow from tidal- and wave-driven circulation of seawater through the beach aquifer, respectively, and D_m represents all other contributors to SGD including meteoric waters (resulting from aquifer recharge) and seasonally discharged seawater as described by Michael et al. (2005).

The outflow seepage rate driven by waves per unit alongshore distance, D_w, can be expressed as follows (Li et al., 1999):

$$D_w = K_h s_w L, \tag{3}$$

where K_h is the hydraulic conductivity of beach sand, S_w is the slope of the wave setup, and L is the surf zone width defined as the distance between the breaker line and the wave runup line. S_w and L can be calculated from the local oceanographic and geologic conditions:

$$s_w = \frac{3\sigma s_b}{8 + 3\sigma^2} \tag{4}$$

and

$$L = \frac{H_b}{\sigma(s_b - s_w)} \tag{5}$$

where H_b is the breaker height, s_b is the beach slope, and σ is the breaking index

$$\sigma = \frac{1.56}{1 + \exp(-19.5 s_b)} - 43.8[1 - \exp(-19 s_b)]\frac{H_b}{g T_w^2}, \tag{6}$$

where T_w is the wave period and g corresponds to gravitational acceleration.

The tidally driven groundwater outflow seepage rate per alongshore distance (D_t) can be estimated as follows (Li et al., 1999):

$$D_t = \frac{n_e A}{\kappa T_t}\exp(-\alpha)[\cos(\alpha) - \sin(\alpha)] + \frac{\sqrt{2n_e}A^2}{s_b T_t}\exp\left(-\sqrt{2\alpha}\right)\cos\left(\sqrt{2\alpha}\right) + \frac{n_e A^2}{s_b T_t} \tag{7}$$

with

$$\kappa = \sqrt{\frac{n_e \omega}{2K_h H}} \tag{8}$$

and

$$\alpha = \frac{kA}{s_b}. \tag{9}$$

In the above equations, A corresponds to the tidal amplitude, T_t the tidal period, ω the tidal frequency, n_e the effective porosity of the beach sand, and H the aquifer thickness.

Input parameters required for application of these models to our study site are given in Table 1. The slope of the beach was reported previously by Boehm (2003). The magnitude of the M_2 tidal harmonic is used for A as is its period (12.42 h) and frequency. According to the Huntington Beach Lifeguard records, breaking wave heights were on average 1 m (David Pryor, California State Parks, person. comm., 2004) during the study. Although records are not kept for wave period, we use 15 s as this is typical for the field site (personal observation). The effective porosity and hydraulic conductivity of the sand were measured in the lab with aquifer material, as described earlier. Komex H_2O Science (2000) reports six measurements of K_h for the unconfined aquifer within 1 km of the field site ranging from 3×10^{-5} to 7.4×10^{-4} m s^{-1}. The geometric mean of the

Table 1
Parameters used for calculation of D_w and D_t

Parameter (units)	Value
H_b (m)	1
T_w (s)	15
g (m^2 s^{-1})	9.81
s_b (−)	0.03
K_h (m s^{-1})	1.5 × 10−4
A (m)	0.5
T_t (s)	44700
ω (rad s^{-1})	1.41 × 10−4
n_e (−)	0.36
H (m)	30.5

K_h is the geometric mean of field observations.

estimates is $K_h = 1.5 \times 10^{-4}\,m\,s^{-1}$. The field measurements were determined with aquifer pumping tests using Theis, Neuman and Distance-Drawdown methods. Because hydraulic conductivity estimates span at least an order of magnitude, we present a sensitivity analysis for K_h, incorporating the possible range of values expected based on lab and field analyses. H is estimated in the same report by Komex H_2O Science for the unconfined aquifer 1000 m inland as 30.5 m. This agrees with subsurface mapping of the field site completed by the California Department of Water Resources (1966).

3. Results and discussion

3.1. ^{226}Ra distribution overview

Fig. 3 shows the spatial distribution of ^{226}Ra activities integrated over alongshore space and time

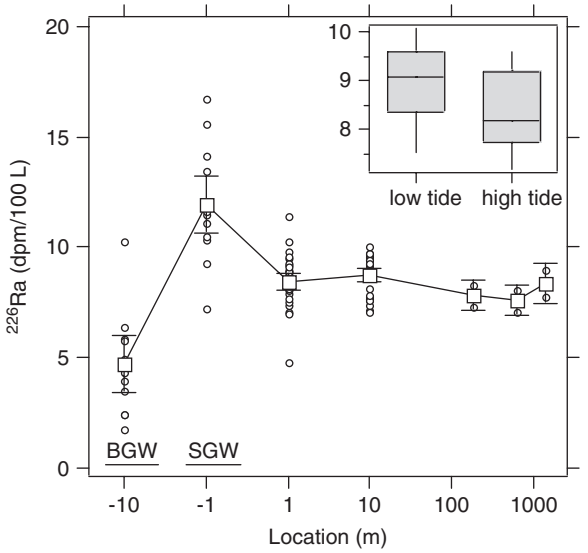

Fig. 3. Average and 90% confidence intervals of ^{226}Ra (open squares and error bars) viewed as a cross-section from the aquifer to the most offshore sampling site, along with raw data (open circles). Spread in data at each site represents variability in space (in the alongshore direction) and time. Samples from the mixing zone (BGW) and intertidal wells (SGW) are shown to the left of the coastal water samples. The location of these inland relative to 0 m is roughly 10 m (intertidal wells) and 50 m (mixing zone wells). The inset shows the range of ^{226}Ra activities measured in the surf zone (locations at 1 and 10 m from large graph) during high and low tides in the form of a "box and whisker plot". The units on the y-axis are the same as those on the main graph (dpm/100 L). The top and bottom of the grey boxes define the 75th and 25th percentiles, respectively. The lines through the middle of the boxes show the medians. The ends of the two "whiskers" define the 90th and 10th percentiles, respectively.

at the field site. The error bars (and errors mentioned in the rest of the paper) represent the 90% confidence intervals given the whole range of tidal variability of ^{226}Ra at each site and not the analytical error. Intertidal wells contained saline groundwater (hereafter referred to as SGW) (average salinity = 33.2 psu) that had significantly ($p<0.1$) higher ^{226}Ra (average of 12.0 ± 1.3 dpm/100 L, $n = 12$) compared to the surf zone samples (average of ankle and waist depth water 8.5 ± 0.4 ($n = 29$) and 8.7 ± 0.3 ($n = 29$) dpm/100 L, respectively). The average salinity of surf zone samples was 33.1 PSU. Samples collected offshore of the surf zone had lower activities relative to the surf zone samples (7.8 ± 0.7 dpm/100 L at 182 m, 7.6 ± 0.7 dpm/100 L at 608 m, and 8.4 ± 0.9 dpm/100 L at 1350 m, $n = 2$ for each average); the average salinity of all offshore samples was 33.2 psu. Although the differences between offshore and surf zone ^{226}Ra activities are not significant when all samples are pooled across the entire month of sampling over various tidal conditions, synoptic measurements during the offshore transects illustrate that there were notable trends of decreasing radium activities with increasing distance from shore (Fig. 4, bottom panel). Interestingly, samples collected at 1350 m offshore showed higher activities than the two offshore samples at 182 and 608 m. This could be explained by the offshore water being of different origin than the nearshore water, perhaps advected from another location. Other possibilities are that it is influenced by a seep or another aquifer discharging radium-rich groundwater offshore, or it is impacted by a potentially radium-rich anthropogenic waste stream released in the vicinity of the field site (thermal and wastewater outfalls shown in Fig. 1—note that radium activities have not been measured in these waste streams).

Groundwater collected from wells in the mixing zone (hereafter referred to as BGW) ranged in salinity from 3.1 to 9.5 psu, and activities of ^{226}Ra were significantly ($p<0.1$) lower (4.7 ± 1.0 dpm/100 L, $n = 12$) than those measured in the SGW from the intertidal zone. These low activities are not surprising given the low salinities that would suppress radium desorption from sediment/soils within the aquifer (Webster et al., 1994).

^{226}Ra activities of Talbert Marsh and Santa Ana River ebb flow (salinities undistinguishable from surf zone salinities) were not significantly different from the activities measured in the surf zone (9.7 ± 1.8 and 8.8 ± 0.7, respectively, $n = 2$ for each

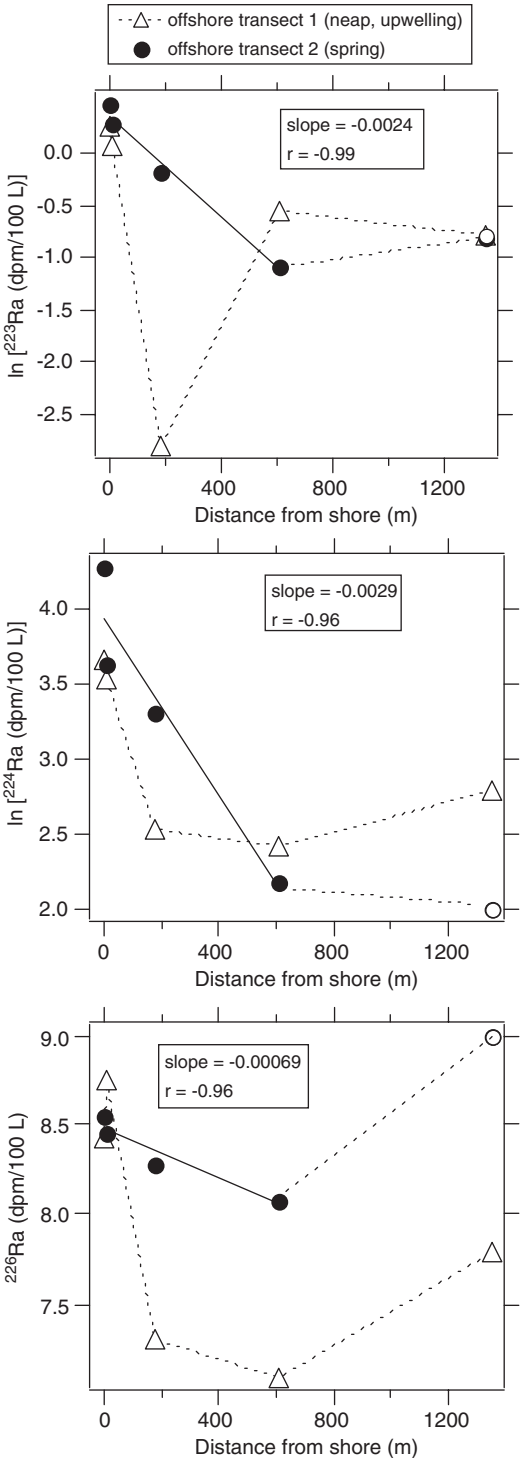

Fig. 4. ln ^{223}Ra, ln ^{224}Ra, and ^{226}Ra as a function of distance in the cross-shore direction. Slopes and correlation coefficients from linear curve fits (solid lines) are reported for data collected during transect 2 within 1 km. Dashed lines connect data from the transects when data are not included in curve fit. Units for slopes are given in text.

average). The two ebb flow samples for each site were obtained during neap and spring tidal conditions. Each time when these sites were sampled, there was at least one surf zone sample that exceeded or was within measurement error of the activities of both ebb flows supporting the conclusion that the ebb flow from these sources was not enriched with radium relative to the surf zone at the time of our study.

The confined Talbert Aquifer (salinity of 16.3 psu) had a ^{226}Ra activity of 944 dpm/100 L, much higher than other ^{226}Ra activities recorded at the field site. The elevated salinity of this water is a result of saltwater intrusion offshore of the field site where the confined aquifer intersects the ocean floor; the precise location where this occurs is not known (T. Sovich, OCWD, personal communication, 2005). As suggested by our conceptual model (Fig. 2), it is conceivable that water from the Talbert Aquifer leaks into the unconfined aquifer through breaches in the aquitard. A previous investigation of the subsurface at the field site suggests that such breaches exist and in some instances, the confined and unconfined aquifers are in direct hydraulic communication (California Department of Water Resources, 1966). We should point out that it is unknown whether water in the Talbert Aquifer directly below or near our sampling sites has a similar radium activity or salinity as the water collected at well M31.

There was not an obvious alongshore gradient in ^{226}Ra activities in the surf zone, SGW, or BGW based on our survey (data not shown). The observed cross-shore distribution of ^{226}Ra activities supports our previous results (Boehm et al., 2004) suggesting discharge of SGW from the unconfined surficial aquifer. An analysis of variance (Matlab, Natwick, MA) between ^{226}Ra activities in the surf zone and tide level (high or low) indicates that activities are significantly ($p<0.1$) elevated during low tides compared to high tides (based on a Kruskal–Wallis non-parametric analysis of variance). This observation points to tidal pumping as an important mechanism for SGD. The reduced offshore gradient in ^{226}Ra activities compared to our previously reported ^{223}Ra and ^{224}Ra activities (Fig. 4) is not surprising since the time scale of mixing and transport in this region is short relative to the extremely long half-life of ^{226}Ra. In addition, the relatively low ^{226}Ra activities, relative to the short-lived isotopes, are likely due to the elemental composition source rock. Specifically, the regeneration rate

of ^{226}Ra in the nearshore coastal aquifer where SGW interacts with uranium and thorium containing soil and rocks is slow; therefore, the standing-stock of desorbable ^{226}Ra is small.

3.2. Groundwater composition

The activity ratios of the ^{223}Ra and ^{224}Ra to ^{226}Ra in the beach aquifer (1.9 and 39, respectively, Fig. 5) are different from the activity ratios in the Talbert Aquifer (0.18 and 2.0, respectively). If radium-enriched waters from Talbert Aquifer were the source of radium to the unconfined beach aquifer, then the ratios would be identical or the short lived isotopes would decay to some extent, effectively lowering the ratios. Since the ratios are higher in the beach aquifer compared to the Talbert Aquifer, the contribution of Talbert Aquifer groundwater to the beach aquifer is probably minimal overall, suggesting that if breaches exist, as shown in Fig. 2, they are small relative to other water inputs to the unconfined aquifer, or that radium adsorbs onto beach sediment, if experiencing a lower salinity regime, as leakage occurs.

We analyzed the hydrogen (δD) and oxygen (δ^{18}O) isotopic composition of a subset of representative water samples to further evaluate the vertical leakage of the Talbert Aquifer to the unconfined beach aquifer. Both BGW from the surficial aquifer and Talbert Aquifer waters fall on a local meteoric line (Yurtsever and Gat, 1981) but have distinct δD and δ^{18}O values (Fig. 6A). δD and δ^{18}O of SGW, on the other hand, cluster close to the seawater values (labeled surf zone and offshore) indicating a significant contribution of seawater. A plot of δ^{18}O versus salinity (Fig. 6B) shows that BGW samples collected from the unconfined aquifer at stations 9 and 10 fall on a mixing line (line 1) between the offshore seawater end member and the lowest salinity BGW sample (collected at station 9). This line has been extended to a hypothetical 0 salinity end member (which was not sampled during the summer of 2003). The isotopic composition of water collected from the mixing zone at station 8, falls on a mixing line (line 2) between the Talbert Aquifer and the hypothetical 0 salinity end-member obtained by extending mixing line 1 to 0 psu salinity. This suggests that BGW collected at station 8 may be composed of nearly 50% Talbert Aquifer water. No samples analyzed fell on the mixing line between the Talbert Aquifer and the seawater end member (line 3). However, it should be pointed out that we did not conduct water isotope analyses on any other samples from station 8.

The fresh groundwater sample collected from station 9 during August of 2005 is shown as a square in Fig. 6B (salinity of 0.1 psu, δ^{18}O of −6.06‰). The sample lays directly at the intersection of mixing lines 1 and 2. If this fresh groundwater sample is representative of fresh groundwater present in the beach aquifer during the summer of 2003 when the rest of the samples were collected, its position on the diagram supports the mixing discussions above. However, there is no way to be certain that the fresh groundwater end member collected in 2005 is the same as one that was present in 2003. This freshwater end-member is likely infiltrated runoff or precipitation.

These results suggest that there is spatial heterogeneity in the composition of waters in the mixing zone of the unconfined aquifer. At stations 9 and 10, waters in the mixing zone (BGW) are composed of seawater and a freshwater end member; the Talbert Aquifer contributes negligibly. At station 8, the BGW may contain a more significant contribution of Talbert Aquifer origin (up to 50%). The results suggest that there may be vertical leakage of the Talbert Aquifer to the unconfined near station 8.

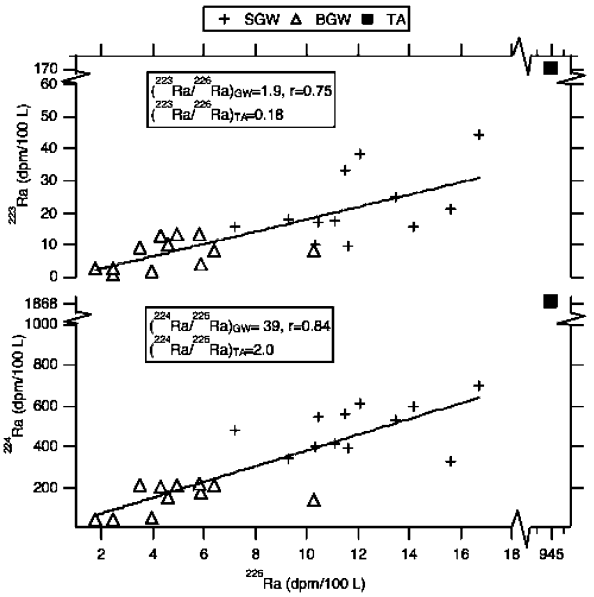

Fig. 5. ^{223}Ra and ^{224}Ra as a function of ^{226}Ra in all groundwater samples (both saline and brackish). Lines represent curve fits between radium isotopes in the unconfined aquifer. There are breaks in the axes to allow viewing of Talbert Aquifer sample. The ratios of radium isotopes are shown for the beach groundwater (GW) and the Talbert Aquifer (TA).

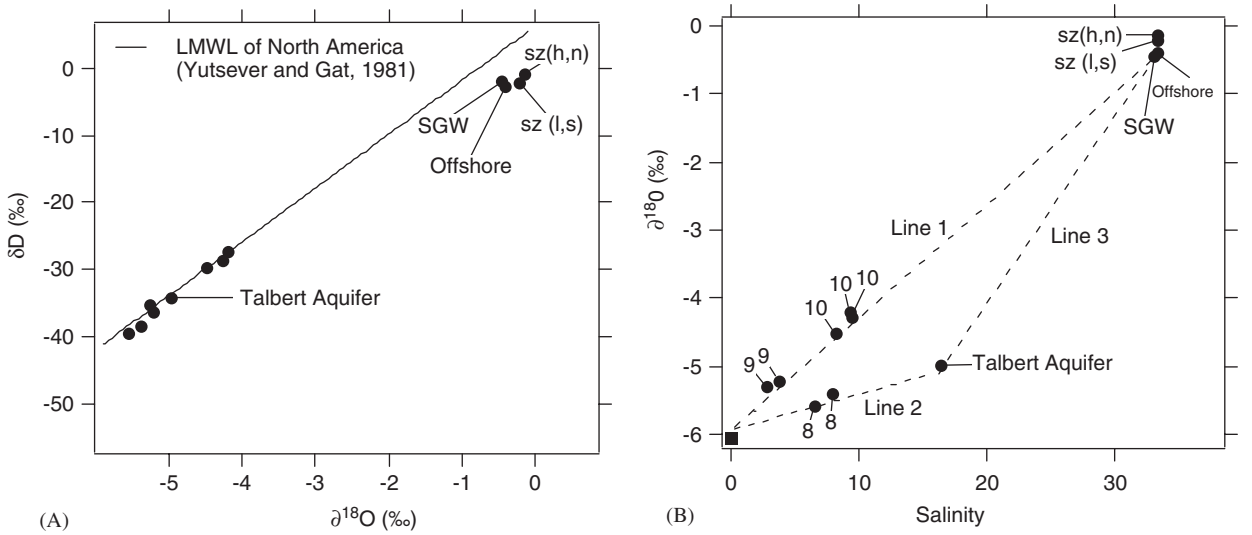

Fig. 6. (A) δD as a function of δ^{18}O in water samples. (B) Mixing diagrams using δ^{18}O and salinity. Each sample is labeled with the location from which it was collected. Numbers refer to the sampling site where brackish groundwater samples were collected; sz(h,n) and sz(l,s) refer to samples collected from the surf zone during high, neap and low, spring tidal conditions, respectively; offshore is the sample collected at the most offshore location during Transect 2; SGW is saline groundwater.

Vertical leakage could occur through a breach in the aquitard, or alternatively, the aquifers could be in direct hydraulic connection in this area (T. Sovich and J. Dadakis, OCWD, personal communication, 2005). Interestingly, the ^{226}Ra activities in BGW from station 8 were not significantly higher than those of BGW collected at other stations, despite the fact that the water isotope data suggests it contains Talbert Aquifer water. This could be because ^{226}Ra re-adsorbs to particle surfaces as it moves from the higher salinity Talbert Aquifer to the lower salinity BGW.

It should be noted that our interpretation of the water isotope data assumes that Talbert Aquifer discharge to the unconfined aquifer has the same salinity and water isotopic composition as Talbert Aquifer at well M31 (approximately 400 m inland, 900 m south-east from the study site). It is possible that the salinity and water isotopic composition spatially vary in Talbert Aquifer in the cross-shore direction as it mixes with seawater (T. Sovich, OCWD, personal communication, 2005), suggesting that the true salinity and isotopic composition of discharge could fall on any value along the mixing line between the Talbert Aquifer and seawater in Fig. 6B (line 3). If the salinity of Talbert Aquifer discharge to the unconfined aquifer near station 8 were much higher than 16 psu, then the BGW at station 8 could no longer be explained as a mixture of the Talbert Aquifer and hypothetical fresh groundwater end members. The presence of another freshwater end-member with lower δ^{18}O would need to be identified to explain the chemistry of BGW at station 8.

3.3. Groundwater flux to the coastal ocean

Fig. 4 (top and middle panels) shows the synoptic offshore oceanic gradients of ln ^{223}Ra and ln ^{224}Ra during the two offshore transects. Transect 1 (open triangles) took place during a neap tide and was coincident with an upwelling event (Boehm et al., 2004). Given that cross-shore advection accompanies upwelling events, the assumption required to derive Eqs. (1) and (2) that cross-shore advection is minimal was violated. Thus, transect 1 was not used to derive mixing coefficients. Transect 2 (open and closed circles) was sampled during a low, spring tide under typical oceanic conditions. The decline in ^{223}Ra and ^{224}Ra follows the Moore (2003) model well within 608 m of the shoreline (Pearson's $r = -0.99$ and -0.96, respectively). The farthest offshore sample at 1350 km had higher radium activities than would be expected due to cross-shore mixing at the rate described by the nearshore decline in radium activities with distance. Moore (2003) also observed a discontinuity in the decline of short-lived radium isotope activities with distance

offshore of the Florida coast and attributed it to different mixing rates in the nearshore relative to offshore. It should be noted that Moore looked at much larger scales than we have examined here (on the order of 10 km offshore). The relatively high offshore activities could be due to an additional source of radium (e.g., discharge from a confined aquifer, a submarine seep, or anthropogenic waste stream) or advection of high radium waters from another location.

To estimate cross-shore eddy diffusivities and the rate of SGD, we use only the activities measured during transect 2, within 1 km of the shoreline, as these are consistent with the model used to derive Eqs. (1) and (2). Using Eq (1), the eddy diffusivity coefficients estimated from ^{223}Ra and ^{224}Ra activities are $K = 0.12$ and $0.26\,m^2\,s^{-1}$, respectively. According to Okubo (1974), K increases as length scale to the $\frac{4}{3}$-power in marine systems. According to the $\frac{4}{3}$ law, at a length scale of 1000 m, K may range from 0.1 to $1\,m^2\,s^{-1}$. Approximately 45 km to the south of the field site in the coastal waters off San Onofre, List et al. (1990) measured K between 2 and $10\,m^2\,s^{-1}$. The K values reported here are within the order of magnitude of the values predicted by the $\frac{4}{3}$ law, but smaller than those reported by List et al. (1990). K surely varies with time at many scales in response to meteorological and oceanographic forcing, thus this estimate should be viewed as an approximation only.

The cross-shore ^{226}Ra gradient ($-6.9 \times 10^{-6}\,dpm\,L^{-1}\,m^{-1}$, Pearson's $r = -0.96$), obtained from a least-squares curve fit of activities measured in transect 2 within 1 km of the shoreline, is shown in Fig. 4 (bottom panel). Applying Eq. (2), the product of the gradient and K estimated from ^{223}Ra and ^{224}Ra yields a ^{226}Ra cross-shore flux of 0.0504 and $0.107\,dpm\,m^{-2}\,min^{-1}$, respectively. The area over which this flux occurs is the vertical cross section of the coastal ocean parallel to shore at the most offshore location (608 m), which in our case is approximately $2814\,m^2$ (assuming 10 m depth 608 m from shore, and an alongshore distance of 281.4 m, bathymetry in Boehm et al., 2002). Thus, the cross-shore flux of ^{226}Ra is estimated at 142 (using ^{223}Ra K) or 300 (using ^{224}Ra K) $dpm\,min^{-1}$. Using the average ^{226}Ra activity of SGW measured in the beach aquifer (12.0 dpm/100 L), this corresponds to a discharge rate per alongshore distance of 4.2 and $8.9\,L\,min^{-1}\,m^{-1}$ (based on estimates of K from ^{223}Ra and ^{224}Ra, respectively). These estimates are within the range reported for the site previously during low, spring tide conditions of $3.1–16\,L\,min^{-1}\,m^{-1}$ using a box model (Boehm et al., 2004).

It should be noted that we have assumed that the ^{226}Ra activity of SGD to the nearshore during the offshore survey is adequately represented by the ^{226}Ra activity of SGW (12.0 dpm/100 L). That is, we have assumed that there is no other important input of groundwater with different ^{226}Ra activities within 608 m of the shore during the survey. This is justified based on the following observations: (1) Boehm et al. (2004) showed that samples collected in the surf zone fell in a mixing line between an offshore end member and SGW based on short-lived radium activities and salinity, suggesting the SGW is a major component of SGD; (2) SGW was observed seeping from the beach (subaerially during extreme low, spring tides) indicating that this water does discharge to the coastal ocean; (3) discharge rates calculated with ^{226}Ra activities from SGW closely match discharge rates obtained from an independent technique (Boehm et al., 2004); and (4) there are no documented groundwater seeps within 608 m of the shoreline (T. Sovich, OCWD, personal communication, 2005). Moore (2003), who originally presented the analysis used in the present work to estimate flux, used ^{226}Ra activities of water captured in a seepage meter at his field site in Florida to calculate the flux of groundwater. Deployment of seepage meters was unreasonable at our study site because of the high degree of wave activity. If there is significant discharge of groundwater along the cross-shore transect that has a variable ^{226}Ra activity relative to SGW, then our estimate for SGD rates could be an under- or overestimate. As will be discussed next, however, the discharge rates we calculated are not only in close agreement with those obtained using an independent method (Boehm et al., 2004) but also are close to what would be expected due to tidal- and wave-driven pumping of seawater through the beach aquifer.

3.4. Model of tidally driven and wave-driven discharge

The models for tidally and wave-driven driven SGD were applied to the study site to determine the proportions of discharge attributable to the outflow portion of wave and tidal pumping of oceanic water and discharge of waters of other origins (e.g., meteoric waters). Based on Eqs. (3) and (7),

and the parameters reported in Table 1 (using the mean in situ measurement of K_h), $D_w = 3.4$ and $D_t = 3.2\,L\,min^{-1}\,m^{-1}$. The sum of these values exceeds the minimum total discharge estimate of $4.2\,L\,min^{-1}\,m^{-1}$ by $2.4\,L\,min^{-1}\,m^{-1}$, and is lower than the maximum estimate of total discharge by $2.3\,L\,min^{-1}\,m^{-1}$. The laboratory measurements of K_h indicated $K_h = 4.7 \times 10^{-4} \pm 2.7 \times 10^{-5}\,m\,s^{-1}$ ($n = 7$). Using this value for K_h in lieu of the one obtained from field estimates, the wave and tide pumped discharge estimates are higher: $D_w = 10.5$ and $D_t = 5.5\,L\,min^{-1}\,m^{-1}$. Both sets of D_w and D_t estimates with realistic K_h predict the rate of SGD due to wave pumping exceeds that due to tidal pumping at this beach, although they are within the same order of magnitude. D_w and D_t estimates based on in situ measurements of K_h at the field site are probably more accurate because removing sediment from an aquifer for laboratory analyses causes resorting and reorganization of the grains which in turn impact the hydraulic conductivity.

Fig. 7 shows D_w, D_t, and their sum ($D_w + D_t$) as a function of K_h. K_h is chosen for our sensitivity analysis because it has the most uncertainty associated with it, with estimates spanning at least an order of magnitude. The x-axis spans the range

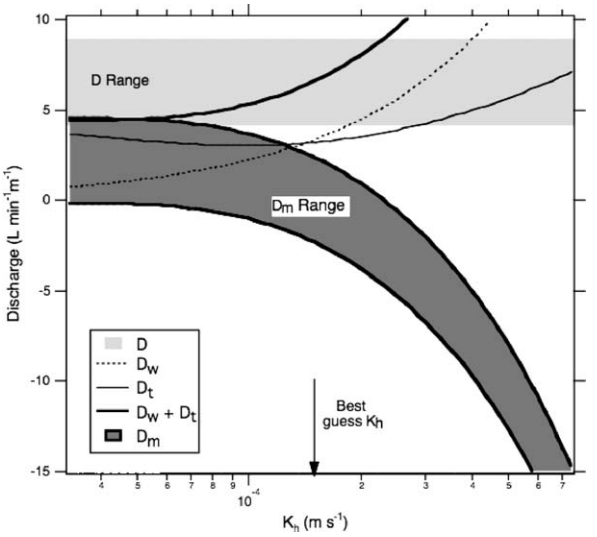

Fig. 7. Discharge due to tides (D_t), waves (D_w), their sum ($D_t + D_w$), and maximum discharge of other waters including meteoric water (D_m, estimated from the difference between the sum of D_t and D_w and the total discharge at the field), as a function of K_h. The light gray horizontal bar denotes the range of discharge calculated from the radium measurements. The x-axis spans the relevant range of K_h at the field site based on laboratory and field measurements.

of K_h relevant to the field site (from 3.3×10^{-5} to $7.4 \times 10^{-4}\,m\,s^{-1}$). The range of estimates for total discharge (D) (4.2–8.9 $L\,min^{-1}\,m^{-1}$) obtained using the estimates of eddy diffusivity and ^{226}Ra gradient is highlighted with light gray. The dark gray band shows the range of estimates for discharge of waters other than wave and tide-pumped seawater (D_m). The band was developed by using both the minimum and maximum D estimates, and assuming D_m makes up the difference between D and $D_w + D_t$. When $D_w + D_t$ exceeds D, D_m is negative indicating that there is some inflow of water to the aquifer that effectively reduces the outflow discharge from the value it would be under the action of waves and tides. On the other hand, if $D_w + D_t$ is less than D, D_m is positive indicating that some component of discharge is not comprised of wave and tide pumped seawater.

If our low-end estimate for D ($4.2\,L\,min^{-1}\,m^{-1}$) is accurate, then negative D_m is predicted for all relevant values of K_h. On the other hand, if our high end estimate for D ($8.9\,L\,min^{-1}\,m^{-1}$) is correct, then D_m is predicted to range from -14 to $4.5\,L\,min^{-1}\,m^{-1}$ over the range of K_h. Given that removal of sediment from an aquifer causes sorting and rearrangement of grains, it is probably more accurate to use the field measurements of K_h in the models for D_w and D_t. Assuming K_h is best approximated with the mean of the field measurements ($1.5 \times 10^{-4}\,m\,s^{-1}$), D_m is predicted to be between 2.4 and $-2.3\,L\,min^{-1}\,m^{-1}$ when D is at the maximum ($8.9\,L\,min^{-1}$ m^{-1}) and minimum ($4.2\,L\,min^{-1}\,m^{-1}$), respectively. This corresponds to 26% and -56% of D, respectively.

Assuming that D_m contains water with low salinities relative to seawater (i.e., freshwater or water originating in Talbert Aquifer), the lack of salinity depression in the coastal ocean suggests that a very low percentage of SGD is not tidally and wave pumped seawater, supporting the low end estimates of D_m that indicate there is salt water intrusion. On the other hand, if D_m consists of water with salinity near that of seawater (i.e., seawater infiltrating and exfiltrating at a seasonal time scale as described by Michael et al., 2005), then the high-end estimate for D_m could be consistent with our salinity observations.

4. Implications for nutrient supply to the surf zone

SGD seepage rates calculated using nearshore eddy diffusion coefficients and ^{226}Ra gradients are

within the rates previously estimated using an independent method (mass balance/box model) (Boehm et al., 2004). At our study site, SGW contains elevated levels of dissolved inorganic nitrogen (DIN, defined as the sum of nitrate and ammonium) and SRP relative to offshore waters with average concentrations of 11.5 and 0.49 μmol L^{-1} (compared to 1.00 and 0.05 μmol L^{-1} offshore), respectively (Boehm et al., 2004). Assuming that nutrient levels in SGW are representative of SGD and given a seepage rate of 7 L min^{-1} m^{-1} of shoreline (the average of our estimates), this implies a discharge of 116 mmol day^{-1} m^{-1} of shoreline DIN and 5 mmol day^{-1} m^{-1} of shoreline SRP. Taking into account that waters offshore contain an order of magnitude less of these nutrients than SGW, discharge induced by tides and waves could be an important source of nutrients to the coastal environment, especially during the dry season. This conclusion is supported by field work along the Gulf of Aqaba in Eilat, Israel (Shellenbarger et al., in review).

The source of nutrients in SGW at the field site is not known. It is possible that dissolved nutrients are supplied by microbial re-mineralization of particulate matter that has infiltrated to the subsurface or regeneration from sediments. Also, elevated levels of DIN (average 343 μmol L^{-1}) and SRP (average 1.2 μmol L^{-1}) concentrations were measured in BGW from the mixing zone (Boehm et al., 2004), just meters from SGW (Fig. 2). We suspect nutrients in BGW emanate from nutrient-polluted (with fertilizer, sewage, and/or detergents) runoff from the surrounding watershed that has infiltrated the subsurface. Even small volumes of BGW mixed into nutrient-depleted SGW could raise nutrient levels over background seawater levels without necessarily causing an obvious salinity depression. Work continues at this field site to explore the origin of DIN via isotopic analysis and nutrient cycling in the subsurface (Santoro et al., in review).

Given that the stretch of open-ocean, sandy shoreline where the study site is located continues for over 20 km, the dry weather delivery of DIN and SRP via SGD is comparable, if not greater, than input of DIN and SRP from the tidal Talbert Marsh and Santa Ana River wetlands to the south-east during similar dry weather conditions. Previous studies documented average summer-time ebb flow rates from the Talbert Marsh of 8.37 m^3 s^{-1} (Grant et al., 2001) and Santa Ana River of 11.57 m^3 s^{-1} (Grant et al., 2002). Because these discharge a small amount of freshwater, and function as tidal wetlands, the discharge values are not expected to change dramatically year to year. Assuming that this flow rate is present during all ebb tides (approximately 12 h day^{-1}), and assuming the DIN and SRP levels measured by us previously (Boehm et al., 2004) are representative of typical conditions (2.54 μmol L^{-1} DIN and 0.1 μmol L^{-1} SRP at the Talbert Marsh and 1.85 μmol L^{-1} DIN and 0.1 μmol L^{-1} SRP at the Santa Ana River), then these watershed outlets deliver to the coastal ocean, together, approximately 1890 mol DIN and 86 mol SRP per day. It should be pointed out that this represents a high-end estimate since the discharge is tidally modulated and is not constant throughout the ebb tides. In addition, some of the ebb flow is recirculated through the wetlands during the following flood tides. Our estimates indicate that DIN and SRP released by these wetlands during the dry season is equivalent to the amount delivered by SGD along 16 km (DIN) and 17 km (SRP) of shoreline. This estimate assumes no alongshore gradients in SGD and nutrient concentrations in SGD.

5. Conclusions

Based on data collected during the summer of 2003, SGD along the shoreline of Huntington Beach is primarily seawater that, under the force of tides and waves, is flushed through the surficial aquifer. We estimate that SGD could be composed of up to 26% water other than wave and tidally pumped seawater. However, our measurements did not identify a salinity depression in the surf zone that could be attributed to BGW discharge, indicating that BGW discharge was not traceable in the coastal ocean with our chemical tools. It is likely that during the wet season, when there is more infiltration of runoff to the unconfined aquifer, that a salinity depression would be observable, and BGW would compose more of the SDG.

Under a set of assumptions, the discharge estimated from radium isotopes is less than that estimated from models of wave and tidally pumped seawater through the aquifer. This result suggests that some of the seawater pumped by tides and waves into the aquifer is not discharged. The forcing mechanism for this influx could be seasonal recharge and evapotranspiration discussed by Michael et al. (2005).

The confined Talbert Aquifer does not appear to contribute significantly to radium (and thus other solutes) in the surficial unconfined beach aquifer at our main study site between stations 9 and 10, based on analyses of radium and isotopic composition of water. However, the water isotope data suggest that Talbert Aquifer communicates with the BGW in the unconfined aquifer at station 8 (to the south-east of our main study area). However, it does not appear to contribute radium. Communication between confined and unconfined aquifers may occur via breaches in the aquitard.

Acknowledgements

The authors acknowledge Billy Moore for constant support and guidance with the radium analyses. Keeney Willis and Keith Loague assisted with the hydraulic conductivity tests. Alyson Santoro and Nick Nidzieko collected the fresh groundwater sample during the summer of 2005. Tim Sovich and Jason Dadakis from the Orange County Water District are acknowledged for stimulating discussions about the data and the Talbert Aquifer. Megan Young, Scott Wankel, and several anonymous reviewers provided comments that improved the manuscript. ABB acknowledges the Clare Boothe Luce Professorship, the Powell Foundation, and the UPS Foundation. AP acknowledges the UPS Urbanization Research Fund.

References

Boehm, A.B., 2003. Model of microbial transport and inactivation in the surf zone and application to field measurements of total coliform in Northern Orange County, California. Environmental Science and Technology 37, 5511–5517.

Boehm, A.B., Sanders, B.F., Winant, C.D., 2002. Cross-shelf transport at Huntington Beach—implications for the fate of sewage discharged through an offshore ocean outfall. Environmental Science and Technology 36, 1899–1906.

Boehm, A.B., Shellenbarger, G.G., Paytan, A., 2004. Groundwater discharge: potential association with fecal indicator bacteria in the surf zone. Environmental Science and Technology 38, 3558–3566.

Buddemeier, R.W. (Ed.), 1996. Groundwater discharge in the coastal zone: Proceedings of an International Symposium. LOICZ/R&S/96-8, iv+179 pp. LOICZ, Texel, The Netherlands.

Cable, J.E., Bugna, G.C., Burnett, W.C., Chanton, J.P., 1996. Application of ^{222}Rn and CH_4 for assessment of groundwater discharge to the coastal ocean. Limnology and Oceanography 41, 1347–1353.

California Department of Water Resources, 1966. Santa Ana Gap Salinity Barrier, Orange County, California. California Department of Water Resources Bulletin No. 174–1.

Charette, M.A., Buesseler, K.O., Andrews, J.E., 2001. Utility of radium isotopes for evaluating the input and transport of groundwater-derived nitrogen to a Cape Cod estuary. Limnology and Oceanography 46, 465–470.

Church, T.M., 1996. An underground route for the water cycle. Nature 380, 579–580.

Cohen, J.E., Small, C., Mellinger, A., Gallup, J., Sachs, J., 1997. Estimates of coastal populations. Science 278, 1209–1213.

Corbett, D.R., Chanton, J., Burnett, W., Dillon, K., Rutkowski, C., Fourqurean, J.W., 1999. Patterns of groundwater discharge into Florida Bay. Limnology and Oceanography 44, 1045–1055.

Elsinger, R.J., Moore, W.S., 1983. ^{224}Ra, ^{228}Ra and ^{226}Ra in Winyah Bay and Delaware Bay. Earth and Planetary Science Letters 64, 430–436.

Epstein, S., Mayeda, T., 1953. Variation of O-18 content of waters from natural sources. Geochemica et Cosmichimica Acta 4, 213–224.

Grant, S.B., Sanders, B.F., Boehm, A.B., Redman, J.A., Kim, J.-H., Mrse, R.D., Chu, A.K., Gouldin, M., McGee, C.D., Gardiner, N.A., Jones, B.H., Svejkovsky, J., Leipzig, G.V., Brown., A., 2001. Generation of enterococci bacteria in a coastal saltwater marsh and its impact on surf zone water quality. Environmental Science and Technology 35, 2407–2416.

Grant, S.B., Sanders, B.F., Boehm, A.B., Arega, G., Ensari, S., Mrse, R., Kang, H., Reeves, R., Kim, J., Redman, J., Jiang, S., Chu, W., Choi, S., Clark, C., Litz, L., Sutula, M., Noblet, J., Sobsey, M., McGee, C., 2002. Coastal Runoff Impact Study (UCI-CRIS), Phase II: sources and dynamics of fecal indicators in the lower Santa Ana River watershed. Technical Report for the National Water Research Institute, Fountain Valley, California.

Johannes, R.E., 1980. The ecological significance of the submarine discharge of groundwater. Marine Ecology Progress Series 3, 365–373.

Kelley, R.P., Moran, S.B., 2002. Seasonal changes in groundwater input to a well-mixed estuary estimated using radium isotopes and implications for coastal nutrient budgets. Limnology and Oceanography 47, 1796–1807.

Kendall, C., Coplen, T.B., 1985. Multisample conversion of water to hydrogen by zinc for stable isotope determination. Analytical Chemistry 57, 1437–1440.

Kim, G., Butnett, W.C., Dulaiova, H., Swarzenski, P.W., Moore, W.S., 2001. Measurement of ^{224}Ra and ^{226}Ra activities in natural waters using a radon-in-air monitor. Environmental Science and Technology 35, 4680–4683.

Komex H_2O Science, 2000. Geophysical, hydrogeologic and sediment investigation as part of the urban runoff/coastal remediation action plan for Huntington Beach, California. Technical Report, The City of Huntington Beach: Huntington Beach, CA.

Krest, J.M., Harvey, J.W., 2003. Using natural distributions of short-lived radium isotopes to quantify groundwater discharge and recharge. Limnology and Oceanography 48, 290–298.

Krest, J.M., Moore, W.S., Gardner, L.R., Morris, J.T., 2000. Marsh nutrient export supplied by groundwater discharge:

evidence from radium measurements. Global Biogeochemical Cycles 14, 167–176.

Li, L., Barry, D.A., Stagnitti, F., Parlange, J.-Y., 1999. Submarine groundwater discharge and associated chemical input to a coastal sea. Water Resources Research 35, 3253–3259.

List, E.J., Gartrell, G., Winant, C.D., 1990. Diffusion and dispersion in coastal waters. Journal of Hydraulic Engineering 116, 1158–1179.

Longuet-Higgens, F.R.S., 1983. Wave set-up, percolation and undertow in the surf zone. Proceedings of the Royal Society London, Series A. 390, 283–291.

Michael, H.A., Mulligan, A.E., Harvey, C.F., 2005. Seasonal oscillations in water exchange between aquifers and the coastal ocean. Nature 436, 1145–1148.

Moore, W.S., 1976. Sampling ^{228}Ra in the deep ocean. Deep-Sea Research 23, 647–651.

Moore, W.S., 1996. Large groundwater inputs to coastal waters revealed by ^{226}Ra enrichment. Nature 380, 612–614.

Moore, W.S., 1997. High fluxes of radium and barium from the mouth of the Ganges-Brahmaputra River during low river discharge suggest a groundwater source. Earth and Planetary Science Letters 150, 141–150.

Moore, W.S., 1999. The subterranean estuary: a reaction zone of ground water and sea water. Marine Chemistry 65, 111–125.

Moore, W.S., 2003. Sources and fluxes of submarine groundwater discharge delineated by radium isotopes. Biogeochemistry 66, 75–93.

Moore, W.S., Krest, J., Taylor, G., Roggenstein, E., Joye, S., Lee, R., 2002. Thermal evidence of water exchange through a coastal aquifer. Geophysical Research Letters 29, [doi:10.1029/2002GL014923].

Nielson, P., 1990. Tidal dynamics of the water table in beaches. Water Resources Res. 26, 2127–2134.

Okubo, A., 1974. Some speculations on oceanic diffusion diagrams. Rapport et Proces-Verbaux des Reunions. Commision Internationale pour L'Exploration Scientifique de la Mer. 167, 77–85.

Paytan, A., Shellenbarger, G.G., Street, H.J., Gonneea, E.M., Davis, K.A., Young, B.M., Moore, W.S., 2006. Submarine groundwater discharge an important source of new inorganic nitrogen to coral reef ecosystems. Limnology and Oceanography 51, 343–348.

Santoro, A.E., Boehm, A.B., Francis, C.A. Denitrifier community composition along a nitrate and salinity gradient in a coastal aquifer. Applied and Environmental Microbiology, in review.

Shellenbarger, G.G., Monismith, S.G., Genin, A., Paytan, A. The importance of submarine groundwater discharge to the nearshore nutrient supply in the Gulf of Aqaba (Israel). Limnology and Oceanography, in review.

Valiela, I., Teal, J.M., Volkmann, S., Shafer, D., Carpenter, E.J., 1990. Nutrient and particulate fluxes in a salt marsh ecosystem: tidal exchanges and inputs by precipitation and groundwater. Limnology and Oceanography 23, 798–812.

Webster, I.T., Hancock, G.J., Murray, A.S., 1994. Use of radium isotopes to examine pore-water exchange in an estuary. Limnology and Oceanography 39, 1917–1927.

Yang, H.S., Hwang, D.W., Kim, G.B., 2002. Factors controlling excess radium in the Nakdong River estuary, Korea: submarine groundwater discharge versus desorption from riverine particles. Marine Chemistry 78, 1–8.

Yurtsever, Y., Gat, J.R., 1981. Atmospheric waters (Chapter 6). In: Gat, J.R., Gonfiantini, R. (Eds.), Stable isotope hydrology in the water cycle. IAEA, Vienna. Technical Report, Series No. 210.